Proceedings of International Structural Engineering and Construction, 7(2), 2020
Emerging Technologies and Sustainability Principles
*Edited by* Askarinejad, H., Yazdani, S., and Singh, A.

ISSN: 2644-108X
www.doi.org/10.14455/ISEC.2020.7(2).GFE-02

# ON THE PARTICLE CRUSHING FEATURES OF SANDY SOILS

HARUYUKI YAMAMOTO

*Division of Development Science, Hiroshima University / IDEC, Higashi-Hiroshima, Japan*

Previous studies have investigated particle crushing of sandy soils in high-pressure conditions. In practice, the volume shrinkage and decreasing shear strength due to particle crushing around the pile-foundation tip in crushable sandy soils may be more important. Therefore, this study aims to confirm the volume shrinkage of sandy soils, e.g., silica sand, weathered granite, and volcanic sand, under various stress paths with a combination of high principal stresses. High-pressure crushing tests were carried out using a true tri-axial compression apparatus under the planned stress paths. Isotropic compression tests and combined stress tests (mean stress $p$ and deviatoric stress $q$) were employed for three types of sandy soil. The particle-crushing progress became active in combination with mean stress $p$ and deviatoric stress $q$. In addition, the relationships between the plastic volumetric strain and relative breakage were found to be approximately linear. As expected, the silica sand was less crushable than the weathered granite sand and volcanic sand under the same stress conditions.

*Keywords*: Tri-axial compression, High pressure, Stress path, Mean stress, Deviatoric stress, Lode angle, Volumetric strain, Deviatoric strain, Plastic work.

## 1 INTRODUCTION

Many experimental and theoretical studies have been conducted to investigate the mechanism of particle-crushing behavior and mechanical characteristic change of sandy soils (Miura and Ohara 1979, Hardin 1985, Fukumoto 1992, Nakata *et al.* 1999). Particle crushing should be especially considered during the design and simulation of the tip-bearing capacity of a pile foundation in crushable sand (Yasufuku *et al.* 2001, Kuwajima *et al.* 2009, Wu *et al.* 2013). The unstable bearing capacity of crushable sandy soil is a particularly severe problem. In previous experimental studies, high-pressure compression and shear tests have been performed using the testing apparatus on sand (Miura and Ohara 1979, Fukumoto 1992, Nakata *et al.* 1999, Yasufuku *et al.* 2001). However, most previous particle-crushing tests were performed under stress conditions involving the usual tri-axial compression, Ko compression, and simple shear.

In this study, a specialized true tri-axial high-compression apparatus, which controls the principal stresses in a three-dimensional stress space, was used for the particle-crushing tests. Three-dimensionally complicated stress distributions have high-stress conditions in the ground near the pile tip. That is, the high-stress distribution directly beneath the center of the pile tip is close to the Ko condition, and the high shear stress is distinguished in the ground near the corner edge of the pile tip.

Further, the crushability of sand is related to its inherent material property and the state of its grain-size distribution. Therefore, silica sand, weathered granite, and volcanic sand are used in the crushing tests, with adjustments to ensure the same grain-size distribution.

## 2 TEST OUTLINE

A specifically-manufactured true tri-axial high-compression apparatus (Yokura *et al*. 2015) was used to control the various stress paths under high-pressure conditions. Figure 1 shows the schematic view of the apparatus. As shown in Figure 2, a cubic test specimen with a 50 × 50 × 50 $mm^3$ edge-cutting shape was installed in the center of this apparatus; a special holder was used to prevent the test sand from leaking. The specimen was loaded using a three-way manual-control electrically powered oil pump and jack, with 200-MPa maximum stress, through the square (40 × 40 $mm^2$) rigid quenched steel loading columns.

Toyoura silica (TS) sand from Yamaguchi Prefecture, weathered granite sand (WG) from Hiroshima Prefecture ("Masado" in local parlance), and volcanic sand (VS) from Kagoshima Prefecture ("Sirasu" in local parlance) were used in this study. They were compacted to an initial relative density of 90% or more. To study the grain size and grain-size distribution effects on sand crushability, other controlled grain sizes, and sand distribution were prepared, in addition to the three types of original sand (TS, WG, and VS), as shown in Figure 3.

Table 1 shows the test numbers corresponding to the grain size distributions in Figure 3; the granularity characteristics of the test sands are taken from the results of preliminary sieving tests ($D_{60}$ indicates the diameter of 60 percent passing particle). It is particularly emphasized that the inherent particle-crushing features can be compared because TS-O, WG-1, and VS-1 have exactly the same grain-size distribution.

The mean stress, $p$, deviatoric stress, $q$, and Lode angle, $\theta$, are controlled independently in this study. It was necessary to make changes only in the stress path while maintaining the values for mean stress $p$ and deviatoric stress $q$. Therefore, experiments were conducted by setting a stress path on the $p$-$q$ and π planes. Figure 4 shows the relationships between the $p$-$q$ and π planes and the three-dimensional principal stresses. Figure 5 shows the stress path on the π-plane.

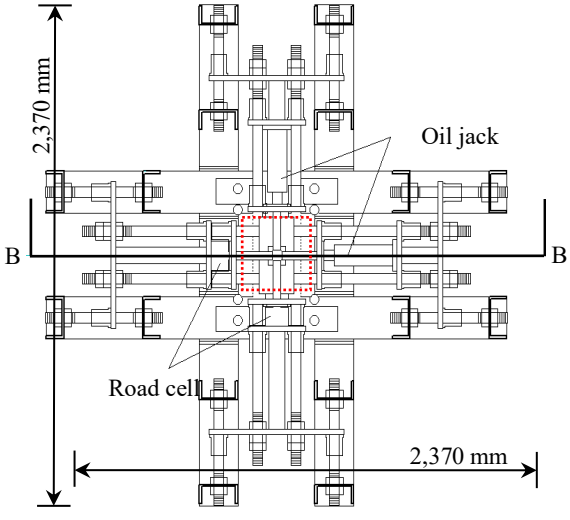


Figure 1. Schematic view of the true tri-axial high -compression apparatus.

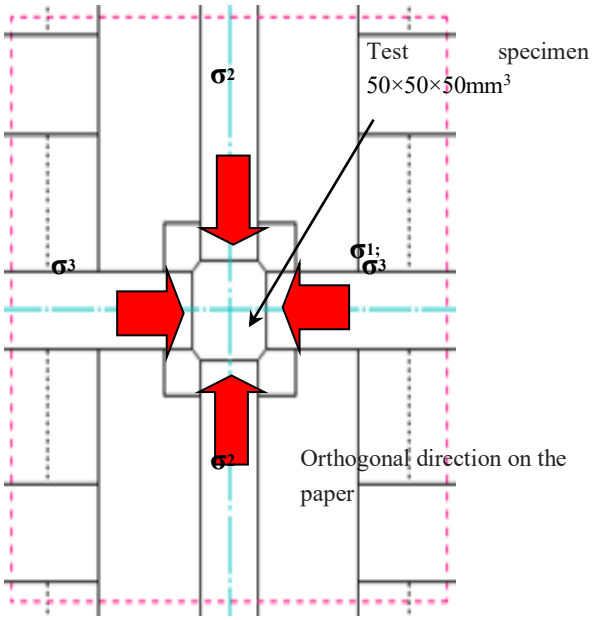


Figure 2. Enlarged view of the dotted-line part in Figure 1.

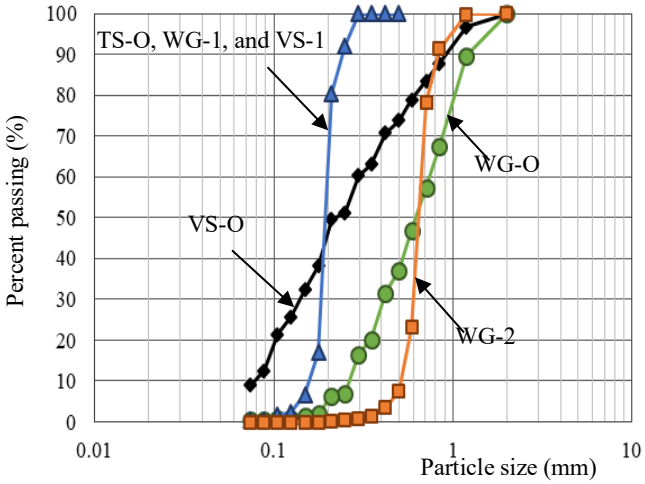


| | |
|---|---|
| TS-O | Toyoura silica sand (Original) |
| WG-O | Weathered granite (Original; Masado) |
| WG-1 | Adjusted to the same grain-size distribution as TS-O |
| WG-2 | Adjusted to the proportionally expanded ( 3.3× ) grain-size distribution of TS-O with the grain-size of (WG-O), $D_{50}$ |
| VS-O | Volcanic sand (Original; Sirasu) |
| VS-1 | Adjusted to the same grain-size distribution as TS-O |

Figure 3. Original and adjusted grain-size distributions of test sands.

Table 1. Granularity characteristics of test sands.

| Test No. | $D_{60}$ (mm) | $D_{50}$ (mm) | $D_{30}$ (mm) | $D_{10}$ (mm) | $U_C$ | $U_C'$ |
|---|---|---|---|---|---|---|
| TS-O | 0.20 | 0.19 | 0.18 | 0.16 | 1.25 | 1.01 |
| WG-O | 0.75 | 0.62 | 0.41 | 0.27 | 2.78 | 0.83 |
| WG-1 | 0.20 | 0.19 | 0.18 | 0.16 | 1.25 | 1.01 |
| WG-2 | 0.67 | 0.62 | 0.60 | 0.52 | 1.29 | 1.03 |
| VS-O | 0.29 | 0.22 | 0.14 | 0.08 | 3.63 | 0.84 |
| VS-1 | 0.20 | 0.19 | 0.18 | 0.16 | 1.25 | 1.01 |

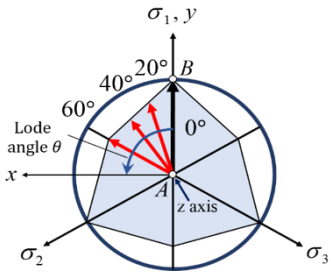


Figure 5. Stress paths on the π plane.

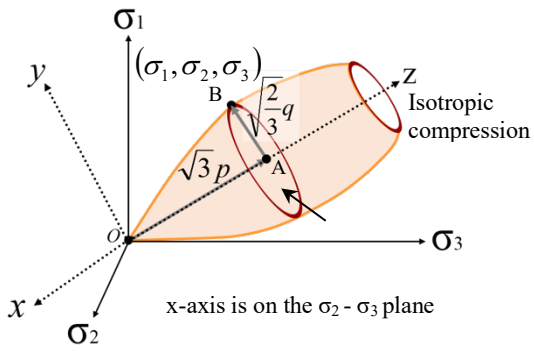


Figure 4. *p-q* and π planes in the three-dimensional principal stress field.

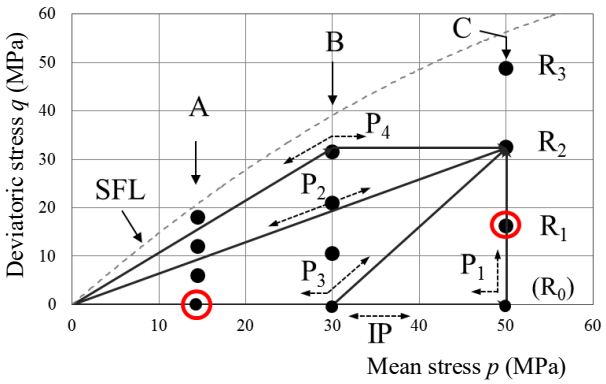


Figure 6. Stress-path patterns on the *p-q* plane.

Mean stress *p* and deviatoric stress q are defined below (see Figure 4).

$$p = \frac{1}{3}(\sigma_1 + \sigma_2 + \sigma_3) \tag{1}$$

$$q = \frac{1}{\sqrt{2}}\sqrt{(\sigma_1 - \sigma_2)^2 + (\sigma_2 - \sigma_3)^2 + (\sigma_3 - \sigma_1)^2} \tag{2}$$

In the case of TS-O, various stress paths were employed to study their effect on particle crushing (Fukuda *et al*. 2018a). The particle-crushing experiments were conducted by setting the stress paths on the *p*-*q* plane, as shown in Figures 5 and 6. First, three π-planes with mean stresses $p$ = 14.5 (A), 30 (B), and 50 (C) MPa are fixed, considering the loading capacity of the apparatus. Experiments were conducted using stress paths with Lode angles $\theta$ = 0°, 20°, 40°, and 60° for each deviatoric-stress levels. The shear failure limit (SFL) condition (stress-path pattern: $P_1$ in Figure 6) and isotropic-compression cases were conducted without deviatoric stress (stress-path pattern: IP in Figure 6). Other crushing tests were conducted on the stress path of the *p*-*q* plane with Lode angles $\theta$ = 0° (stress-path patterns: $P_2$, $P_3$, and $P_4$ in Figure 6).

The experimental results of particle-crushing tests under various Lode angles $\theta$ showed that Lode angles $\theta$ had little influence on the crushing property (Fukuda *et al*. 2018b). The relative breakage, $B_r$, (Hardin 1985) and plastic work, $W_p$, increased in proportion to the combination of mean stress $p$ and deviatoric stress $q$, with almost no relation to the stress-path patterns in the monotonic loading. Therefore, the IP and $P_1$ stress-path patterns in Figure 6 were employed only for the crushing tests of WG-O, WG-1, WG-2, VS-O, and VS-1 in this study.

## 3 TEST RESULTS AND DISCUSSION

First, sieving tests were conducted to determine the particle-size distribution after particle crushing, and relative breakages $B_r$ were fixed. The plastic work, $W_p$, can be calculated by summing the area of each loop of the volumetric-strain, $\varepsilon_v$ - $p$, and deviatoric-strain, $\varepsilon_d$ - $q$, relationships. In addition, the plastic volumetric and deviatoric strains and the elastic volumetric and deviatoric strains were determined in these relations. Because this plastic volumetric strain, $\varepsilon_v^p$, is closely related to the residual volume reduction of the sample, the relationship between the plastic volumetric strain, $\varepsilon_v^p$, and relative breakage, $B_r$, will be discussed.

Figures 7, 9, and 11 show the $B_r$-$W_p$ relationships for TS, WG, and VS, respectively. Figures 8, 10, and 12 show the $B_r$ - $\boldsymbol{\varepsilon_v^p}$ relationships for TS, WG, and VS, respectively. Unique relationships appear, as $B_r$, $W_p$, and $\boldsymbol{\varepsilon_v^p}$ are irreversible amounts. The nearly linear relationship of $B_r$ - $\boldsymbol{\varepsilon_v^p}$ draws special attention.

In a previous study (Fukuda *et al*. 2018a), empirical Eq. (3) was introduced to correlate the relative breakage, $B_r$, mean stress, $p$, and deviatoric stress, q. Figures 13, 14, and 15 show the estimation accuracies of $B_r$ for TS-O, WG-O, 1, and 2, and VS-O, and 1, respectively. In Table 2, the unknown parameters ($A_0$, $r_c$, and c) were fixed using the least-squares method.

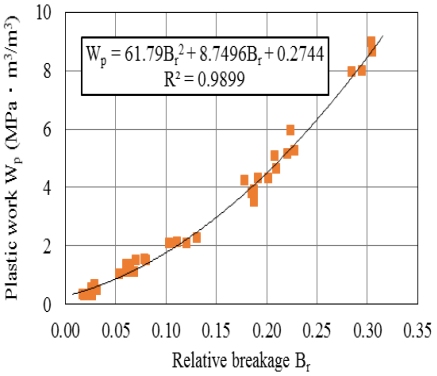


Figure 7. Relationship of $B_r$-$W_p$ for TS-O (stress-path pattern; IP+$P_1$).

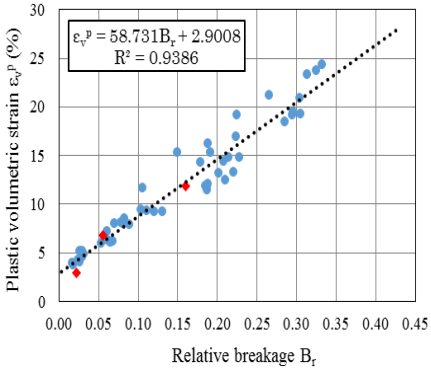


Figure 8. Relationship of $B_r$ - $\varepsilon_v^p$ for TS-O (stress- path pattern; IP+$P_1$).

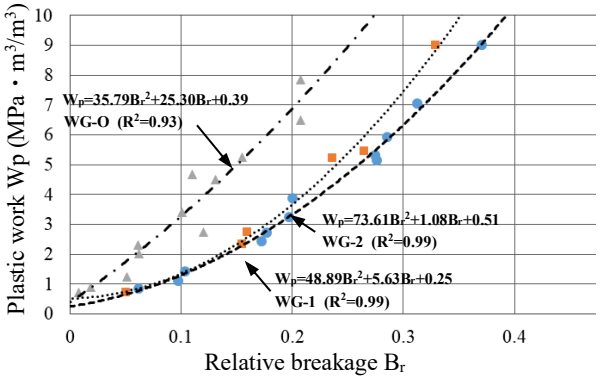


Figure 9. Relationship of $B_r$ -$W_p$ for WG-O, WG-1, and WG-2.

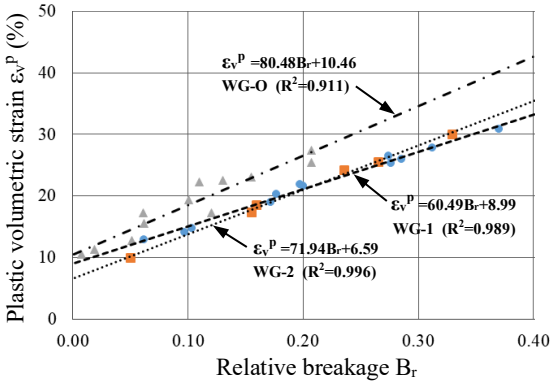


Figure 10. Relationship of $B_r$ - $\varepsilon_v^p$ for WG-O, WG-1, and WG-2.

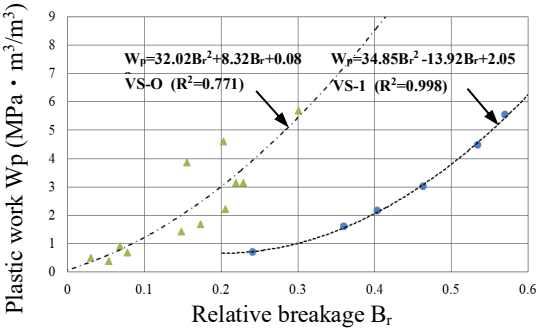


Figure 11. Relationship of $B_r$ -$W_p$ for VS-O and VS-1.

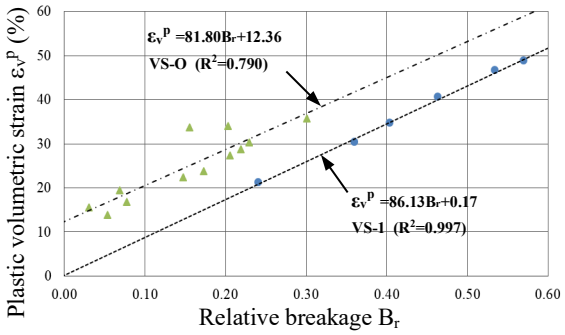


Figure 12. Relationship of $B_r$ - $\varepsilon_v^p$ for VS-O and VS-1.

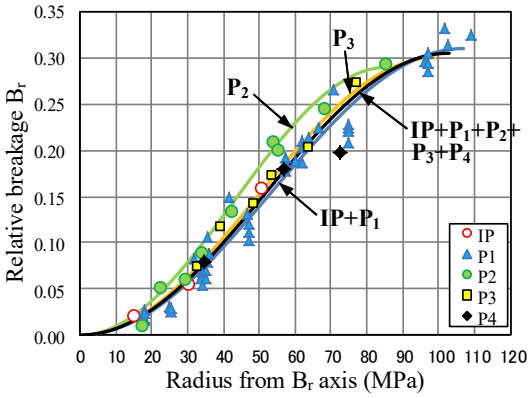


Figure 13. Estimation accuracy of $B_r$ (TS-O).

Table 2. Estimated unknown parameters.

| Test No. | $A_0$ | rc (MPa) | C | $R^2$ | Total number of test |
|---|---|---|---|---|---|
| TS-O ($IP+P_1$) | 0.301 | 107 | 1.70 | 0.974 | 51 |
| WG-O | 0.210 | 78 | 1.10 | 0.740 | 12 |
| WG-1 | 0.350 | 68 | 1.20 | 0.980 | 12 |
| WG-2 | 0.340 | 73 | 1.40 | 0.850 | 6 |
| VS-O | 0.260 | 34 | 1.00 | 0.700 | 12 |
| VS-1 | 0.600 | 25 | 1.04 | 0.750 | 6 |

$$B_r = A_0 \times \left\{1 - \cos\left(\frac{\pi}{2} \times \frac{r}{r_c}\right)\right\} \quad , \quad r^2 = p^2 + (c \times q)^2 \tag{3}$$

The following assumptions were made: $B_r = 0$ when $p = q = 0$; the limit of $B_r$ exists as "$A_0$" at $r = r_c$; the effects of $p$ and $q$ on particle crushing can be estimated as root-mean-square "r"; the effectiveness level is considered to be "c"; the relationship between $B_r$ and r is expressed as the cosine function; and the effects of the stress-path patterns can be neglected.

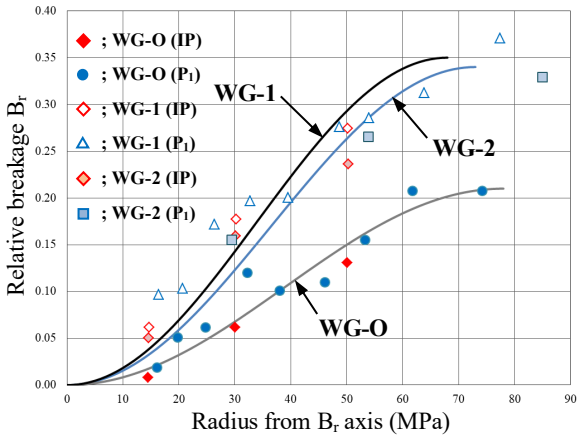


Figure 14. Estimation accuracy of $B_r$ (WG-O,1,2).

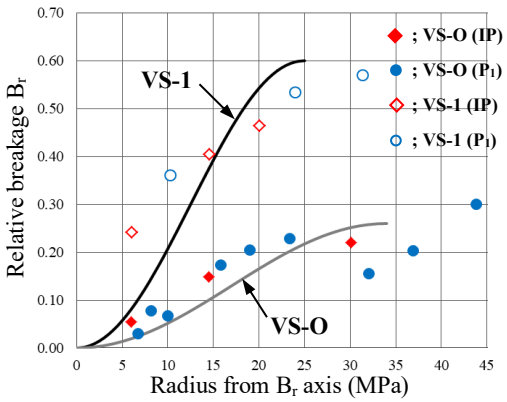


Figure 15. Estimation accuracy of $B_r$ (VS-O,1).

Although some scattered data are found in these figures, the orders of approximation are quite good from an engineering point of view, and the relative breakage, $B_r$, can be directly estimated using these relational expressions with $p$ and $q$. In addition, the plastic volumetric strain, $\varepsilon_v^p$, which is closely related to the residual settlements, can be determined using the estimated $B_r$.

## 4 CONCLUSIONS

In this experimental study, unique relationships were found between $W_p$, $\varepsilon_v^p$, and $B_r$ for three types of sandy soil. Based on the experimental results, specific approximate expressions of the $B_r$ - ($p$, $q$) relationships were derived for three types of sandy soil. Subsequently, $W_p$ and $\varepsilon_v^p$ could also be estimated, considering the stress state of ($p$, $q$) for each sandy soil, using the $B_r$ - $W_p$ and $B_r$ - $\varepsilon_v^p$ relationships.

## References

Fukuda, K., and Yamamoto, H., *Crushing Characteristic of Soil Particle on The Effect of Stress Path*, Streamlining Information Transfer between Construction and Structural Engineering, ASEA SEC-4, GFE-2, December, 2018a.

Fukuda, K., and Yamamoto, H., *On the Effect of Deviatoric Stress for Particle Crushing (in Japanese),* Summaries of Technical paper of Annual Meeting, Architectural Institute of Japan, Structure I, No.20248, September, 2018b.

Fukumoto, T., *Particle Breakage Characteristics of Granular Soil*, Soils and Foundations, Japanese Geotechnical Society, 32(1), 26-40, February, 1992.

Hardin, B. O., *Crushing of Soil Particles*, Journal of Geotechnical Engineering, 111(10), 1177-1192, 1985.

Kuwajima, K., Hyodo, M., and Hyde, A. F. L., *Pile Bearing Capacity Factors and Soil Crushability*, Journal of Geotechnical and Geoenvironmental Engineering, 135(7), 901-913, 2009.

Miura, N., and Ohara, S., *Particle-Crushing of a Decomposed Granite Soil under Shear Stresses*, Soils and Foundations, Japanese Geotechnical Society, 19(3), 1-14, June, 1979.

Nakata, Y., Hyde, A.F.L., Hyodo, M., and Murata, H., *A Probabilistic Approach to Sand Particle Crushing in the Triaxial Test*, Geotechnique, The Institution of Civil Engineers, May, 49(5), 567-583, 1999.

Wu, Y., Yamamoto, H., and Yao, Y. P., *Numerical Study on Bearing Behavior of Pile Considering Sand Particle Crushing*, Geomechanics and Engineering, 5(3), 241-261, 2013.

Yasufuku, N., Ochiai, H., and Ohno, S., *Pile End-Bearing Capacity of Sand Related to Soil Compressibility*, Soils and Foundations, Japanese Geotechnical Society, 41(4), 59 -71, August, 2001.

Yokura, K., Yamamoto, H., and Wu, Y., *Crushing Tests of Soil Particles by High Pressure True Tri-Axial Compression Apparatus*, The 6th Japan-China Geotechnical Symposium, Sapporo, Japan, 51-56, 2015.